Elastoplastic solutions to predict tunnelling-induced load redistribution and deformation of surface structures

Andrea Franza[1] and Matthew J. DeJong[2]

[1]Research Associate in Civil Engineering, Department of Engineering, University of Cambridge, Cambridge, UK. Email: andreafranza@gmail.com

[1]Senior Lecturer in Structural Engineering, Department of Engineering, University of Cambridge, Cambridge, UK. Email: mjd97@eng.cam.ac.uk

ABSTRACT

In this paper, an elastoplastic two-stage analysis method is proposed to model tunnelling-induced soil-structure interaction and incorporated into a computer program 'ASRE'. This solution allows considering both vertical and horizontal greenfield ground movements, gap formation and slippage, continuous or isolated foundations, and a variety of structural configurations and loading conditions. After introducing the proposed formulation, the model predictions are first compared with previously published data for validation. Then, to isolate the effects of various structural characteristics (relative beam-column stiffness, presence of a ground level slab, column height, number of storeys) and foundation types (continuous versus isolated), several example structures are analysed. Results demonstrate the value of the proposed analysis method to study a broad range of building characteristics very quickly, and show how the soil-structure interaction occurring due to underground excavations is altered by both foundation and superstructure configurations. In particular, the difference in behaviour between equivalent simple beams and framed structures on separated footings is clarified.

INTRODUCTION

In urban areas, to satisfy the needs for further underground transportation and services, new tunnels are often excavated near existing structures. As part of the tunnelling design project, engineers need to assess displacements and deformations of existing surface structures resulting from tunnel-structure interaction (TSI). Despite several studies and detailed guidance for risk assessment of continuous foundations and masonry buildings, less attention has been paid to bridges, framed structures, and to foundation schemes with ground level piers/columns on separated footings.

The focus of the work is on the development of a routine design tool to preliminary investigate tunnel-structure interaction that is able to account for the structure/foundation characteristics and to directly implement greenfield inputs while relying on a limited number of rational parameters. Both continuous foundations and separated footings are considered, with the objective of a more comprehensive understanding of the differences in structural behaviour between façade and framed structures. An elastoplastic two-stage analysis method is adopted to estimate structural displacements that result from the tunnel excavation, as well as gap formation and slippage between the foundation and the soil. Firstly, the work focuses on displacements of simple beams in continuous contact with the soil that result from the tunnel excavation; gap formation and slippage beneath the foundation are assessed. Secondly, the effect of the type of foundation is considered by investigating simple beams on separated footings. Then, for the case of separated footings, the structural configurations are progressively varied from a simple beam to simple frames with different structural properties. To compare structural behaviour, load redistribution mechanisms and structural deformation parameters are presented.

BACKGROUND

To assess potential damage to existing buildings caused by the construction of new tunnels, engineers typically adopt a procedure which consists of stages of increased detail and complexity (Mair et al. 1996). [i] Firstly, greenfield ground movements (i.e. predicted ground movements where no structures are present) are used to estimate the potential for damage. A simple prediction of tunnelling-induced ground movements, depending on a limited number of input variables, is possible using empirical methods (Mair et al. 1996; Marshall et al. 2012). Provided greenfield movements are below a certain threshold, structural damage is not a concern. [ii] If greenfield movements exceed a certain threshold, deformations of bearing wall structures on continuous foundations are assessed by imposing the greenfield movements at the structure base. This is typically a conservative method because it neglects that the structural stiffness generally tends to decrease the structural distortions (Franzius et al. 2006; Farrell et al. 2014; Ritter et al. 2017); structural service loads may occasionally increase excavation-induced settlements and associated deformations (Bilotta et al. 2017; Giardina et al. 2015). [iii] If strains within the building are greater than serviceability limits, the building stiffness should be taken into account. Either the modification factor approach, consisting of multiplying the deformations computed with respect to the greenfield movements profiles by a factor that depends on the relative soil-structure stiffness (Franzius et al. 2006), or numerical models of the entire soil-structure domain are used to assess the deformations (Boldini et al. 2018; Fargnoli et al. 2015; Fu et al. 2018; Giardina et al. 2015). However, for foundations consisting of separated footings, it is not clear if directly applying greenfield movements or using previously defined modification factors (mostly developed for buildings on continuous foundations) are acceptable design approaches. Consequently, when analysing structures that are not bearing wall structures on continuous foundations, engineers need to perform numerical models at preliminary design stages. To limit computational costs, the complexity of the numerical model may be decreased by simplifying the superstructure to an equivalent elastic solid (Losacco et al. 2014; Pickhaver et al. 2010) or adopting two-stage solutions based on Winkler and continuum modelling of the soil (the latter approach is investigated in this paper).

A number of studies demonstrated that elastic and elastoplastic methods based on relatively simple continuum and Winkler-based models may provide useful insights for tunnelling beneath pipelines and pile foundations (Klar et al. 2005; Klar et al. 2007; Kitiyodom et al. 2005; Franza et al. 2017). However, these methods have not been exploited to study the deformations of surface structures. Deck and Singh (2012) and Basmaji et al. (2017) developed, respectively, closed-form Winkler and Pasternak based solutions to analyse a simple beam in fully sagging or hogging zone subjected to a roughly circular settlement trough. Although they accounted for the effect of building weight and predict bending deformation reduction due to structure stiffness, the applicability of their analytical methods is limited by the simplified greenfield input and the use of an equivalent simple beam structure. In addition, although linear elastic Winkler springs (i.e. independent vertical springs) are commonly used in structural engineering for the design of foundations, this approach is an approximation of the elastic continuum solution. For instance, Vesic's subgrade modulus was defined to match the maximum bending moments due to a concentrated vertical load of an infinite beam that rests on either Winkler springs or an elastic half-space (Klar et al. 2005; Vesic 1961). Thus, the Winkler subgrade modulus is not only a property of the soil, it depends on both the soil elasticity parameters (Young's modulus, Poisson's ratio), the structure stiffness, loading, and foundation scheme. In contrast, this paper proposes a continuum solution for the soil (with interactive/coupled springs) that is only dependant on the soil elasticity parameters.

ELASTOPLASTIC SOLUTION FOR TUNNEL-STRUCTURE INTERACTION ANALYSIS

Analysis method

To model the tunnel-soil-structure with a simple solution able to account for the structure and foundation configurations, structure stiffness, and service loads while considering gap formation and slippage at the foundation-soil interface, the two-stage solution framework proposed by Klar et al. (2007) and Leung et al. (2010) was used. As illustrated in Figure 1, it is based on the assumption that the elastic surface structure is constrained to a homogeneous elastic continuum through sliders which are rigid-perfectly plastic elements with upper and lower limit forces. The homogeneous elastic continuum is modelled with coupled vertical and horizontal springs that interact with each other. Slippage and gap formation are modelled by decoupled sliders in the horizontal and vertical directions, respectively (the structure is always connected to the soil by the sliders as displayed in Figure 1(b)). Two-dimensional structures composed of Euler-Bernoulli elastic beams are implemented, whereas self-weight and service loads are modelled by uniform loads distributed at the beam axes of the superstructure. The structure is assumed orthogonal to the longitudinal tunnel axis. Furthermore, greenfield movements are evaluated in plane-strain condition and are representative of the final steady-state condition obtained at the conclusion of the tunnel excavation; this paper does not investigate the three-dimensional response of the structure during tunnel heading advancement. The terms ‘structure’, ‘foundation’, ‘superstructure’ are used to indicate, respectively, the entire structure and foundation system, the structural elements in contact with the soil, and the remaining portion of the structure connected to the foundation (see Figure 1).

The two-stage analysis method consists of [1] the evaluation of the greenfield displacement field due to tunnelling, and [2] the analysis of the structure on plastic sliders connected to springs that are subjected to the ground movements calculated from [1]. This two-stage approach is based on the assumptions that the structure does not influence tunnelling and the continuum response to loading is not affected by the tunnel. These assumptions lead to neglect part of the interaction mechanism; however, as discussed in later sections, the induced error may be considered secondary for surface structures.

The solution, implemented into the computer program Analysis of Structural Response to Excavation (ASRE), was achieved numerically using a finite element method (FEM) and a condensed stiffness matrix approach considering the degrees of freedom (vertical and horizontal displacements, and rotations) of the foundation, which consists of either separated footings or a continuous beam. The foundation was discretised in finite elements and the problem was solved through the following global equilibrium equation.

$$\mathbf{S}\mathbf{u} = \mathbf{P} + \mathbf{F} \tag{1}$$

where $\mathbf{S}$ is the condensed stiffness matrix of the structure, $\mathbf{u}$ is the displacement vector of the foundation, $\mathbf{P}$ is the external loading vector of the foundation, and $\mathbf{F}$ is the vector of reaction forces applied by the soil to the foundation nodes. Because of the condensed stiffness approach, $\mathbf{S} = \mathbf{K}_{su} + \mathbf{K}_{fd}$, where $\mathbf{K}_{fd}$ is the stiffness matrix of the foundation and $\mathbf{K}_{su}$ is the condensed stiffness matrix of the superstructure. If all the degrees of freedom (DOFs) of the superstructure base are fixed, an element of the condensed stiffness matrix $K_{su,ij}$ represents the superstructure reaction force in the i^{th} DOF due to a unit displacement of the j^{th} DOF, where i and j represent the DOFs of the frame base contained in the vector u. **P** includes gravity loads of the foundation as well as the condensed form of the gravity and service loads transferred to the foundation by the superstructure (calculated by assuming a fixed base condition for the loaded superstructure).

Because of the compatibility condition, the displacement vector of the foundation, **u**, is given by

$$\mathbf{u} = \mathbf{u}^c + \mathbf{u}^{ip} \tag{2}$$

in which $\mathbf{u}^c$ is the soil continuum displacements and $\mathbf{u}^{ip}$ the plastic interface displacements. The soil continuum displacements, $\mathbf{u}^c$, is related to the soil flexibility matrix $\boldsymbol{\Lambda}$ (in which the generic component Λ_{ij} describes the soil displacement at node i induced by a unit force applied at node j) by the vector containing the forces acting on the entire soil medium. In the case of tunnelling, these forces are due to both tunnel excavation and the superstructure. If only the degrees of freedom of the base of the foundation are considered, the continuum displacement can be written as

$$\mathbf{u}^c = \mathbf{u}^{cl} + \mathbf{u}^{cap} + \mathbf{u}^{cat}; \qquad \mathbf{u}^{cl} = \boldsymbol{\Lambda}^l \mathbf{f} \quad \text{and} \quad \mathbf{u}^{cap} = \boldsymbol{\Lambda}^* \mathbf{f} \tag{3}$$

where **f** is the vector containing the forces acting on the soil medium, $\mathbf{u}^{cl}$ is the continuum local displacement due to loading at its location, $\mathbf{u}^{cap}$ is the additional continuum displacements due to the interaction (i.e. displacement at a given point due to forces acting at other locations), $\mathbf{u}^{cat}$ is the additional displacement due to tunnelling, $\boldsymbol{\Lambda}^l$ is the diagonal matrix of $\boldsymbol{\Lambda}$ (off-diagonal elements are all zero), and $\boldsymbol{\Lambda}^*$ is the soil flexibility matrix without the main diagonal. Because of the principle of action-reaction forces:

$$\mathbf{F} = -\mathbf{f} = -\left(\boldsymbol{\Lambda}^l\right)^{-1} \mathbf{u}^{cl} = -\mathbf{K}^* \mathbf{u}^{cl} \tag{4}$$

where $\mathbf{K}^* = \left(\boldsymbol{\Lambda}^l\right)^{-1}$ is the local stiffness matrix of the soil (i.e. the inverse matrix of the diagonal term of $\boldsymbol{\Lambda}$).

By introducing Equations (2) and (4) in Equation (1) and considering the sliders, equilibrium

Equations (5)-(7) are obtained:

$$(\mathbf{S} + \mathbf{K}^*)\,\mathbf{u} = \mathbf{P} + \mathbf{K}^*\mathbf{u}^{cat} + \mathbf{K}^*\mathbf{\Lambda}^*\,\langle(\mathbf{P} - \mathbf{Su})\rangle + \mathbf{K}^*\mathbf{u}^{ip} \tag{5}$$

$$\langle(\mathbf{P} - \mathbf{Su})\rangle_i = f_{i,low} < (\mathbf{P} - \mathbf{Su})_i < f_{i,up} \tag{6}$$

$$\langle(\mathbf{P} - \mathbf{Su})\rangle_j = |(\mathbf{P} - \mathbf{Su})_j| < \mu\,(\mathbf{P} - \mathbf{Su})_i \tag{7}$$

where $f_{i,up}$ and $f_{i,low}$ are the limit loads of the vertical plastic sliders, μ is the friction coefficient between the soil and foundation, i and j are the translation degrees of freedom in the z and x direction of the n^{th} node, respectively. If downward displacement is defined as positive, $f_{i,low}$ (≤ 0) is the uplift capacity of the soil and $f_{i,up}$ (≥ 0) is the down-drag capacity. Furthermore, at a given node, the frictional condition given by Equation (7) results in the horizontal limit force being greater than zero only if the corresponding vertical spring is in compression. In this paper, for the sake of limiting the number of soil input parameters, $f_{i,low} = 0$ and $f_{i,up} = \infty$. Therefore, in the vertical direction, linear elastic behaviour was implemented with infinite compressive strength and no tensile strength. A fully elastic solution representative of perfect soil-structure bonding could be obtained by imposing $\mathbf{u}^{ip} = 0$ (i.e. by removing horizontal and vertical sliders), as discussed by Franza and DeJong (2017).

With respect to the soil, a homogeneous half-space continuum represented with coupled springs was considered. Adopting an elastic soil with a unique secant Young's modulus representative of the considered tunnelling scenario is consistent with the modification based approach given by Potts and Addenbrooke (1997). However, as discussed by Potts and Addenbrooke (1997) and Mair (2013), it is important to estimate the reasonable order of magnitude of the soil Young's modulus E_s by accounting for the average elastic modulus of the soil above the tunnel and the soil stiffness degradation with strain level (depending on the tunnel volume loss); for a uniform soil, the representative E_s may be estimated as the soil stiffness at half of the depth of the tunnel axis. To model the response of the elastic continuum, the components of the matrix $\mathbf{\Lambda}$ (both diagonal and off-diagonal terms) were obtained on the basis of the elastic integrated forms of Mindlin's solutions given by Vaziri et al. (1982) by assuming a uniform pressure and tangential stress area corresponding to each node of the foundation.

In this study, both purely elastic and elastoplastic solutions of the global tunnel-soil-structure interaction were calculated, which are referred to as 'EL' and 'EP', respectively. Note that under the assumptions of the EL analysis method, the displacements induced by tunnelling and building self-weight would not affect each other, whereas the structure weight does influence the tunnelling-induced displacements, and therefore the structural deformations, calculated with the EP solution. Furthermore, the EL set of equations can be directly solved, whereas EP requires the incremental and iterative procedure described as follows. Firstly, the equilibrium equation is solved for incremental variation of the load vector $\mathbf{P}$, $\Delta\mathbf{P}$, assuming no tunnelling-induced movements ($\mathbf{u}^{cat} = 0$) to obtain the displacement vector $\mathbf{u}^{p}$. Then, for the given total value of $\mathbf{P}$, the incremental displacement solutions corresponding to increments of tunnelling-induced movements, $\Delta\mathbf{u}^{cat}$, are computed. During this second stage, solution $\mathbf{u}$ is calculated, thus tunnelling-induced foundation movements are given by $\mathbf{u}^{tun} = \mathbf{u} - \mathbf{u}^{p}$. In particular, for each increment modelling the variation in the boundary conditions (loads or tunnelling-induced displacements), the numerical iterative single-loop procedure described by Klar et al. (2007) was adopted to obtain the solution displacements. Finally, the foundation displacement vector, $\mathbf{u}$, can be partitioned as follows $\mathbf{u}^{T} = \begin{bmatrix} \mathbf{u}_{su} & \mathbf{u}_{fd} \end{bmatrix}$ to distinguish between the nodes connected to the superstructure, $\mathbf{u}_{su}$, and the remaining nodes of the foundation, $\mathbf{u}_{fd}$. Therefore, superstructure deformed shape and reaction forces can be computed by displacing its base by the sub-vector $\mathbf{u}_{su}$. In the following, the notation u_x and u_z is used to indicate, respectively, horizontal and vertical greenfield soil movements ($\mathbf{u}^{cat}$) and tunnelling-induced foundation displacements ($\mathbf{u}^{tun}$).

Studied configurations

Figure 2 shows the geometry of the tunnel, the considered structural configurations, used nomenclature, and the adopted sign convention (for displacements and forces). Five structural cases were implemented: a simple beam (representing a bearing wall structure) either on continuous footings (STR) or on separated footings (BE), a single-storey frame building supported by either separated footings (FR) or footings connected by a floor slab (FRB), and a bridge on separated footings (BR). Framed configurations have fixed beam-column/pier and column/pier-footing connections. Footings consist of a transverse group of uniformly spaced elements that are rectangular in plan; they rest on the ground surface (i.e. the effects of foundation embedment are not considered).

Greenfield displacement input

Tunnel excavation results in ground movements at the surface that are generally related to ground condition, tunnel depth, z_t, tunnel radius, R, and tunnel volume loss, $V_{l,t}$, which is the ratio between the tunnel ground loss and the notional final area of the tunnel cross-section. It should be noted that the soil volume loss, $V_{l,s}$, which is the settlement trough area normalised by the tunnel area, may differ from $V_{l,t}$ in drained conditions due to soil volumetric strains. Greenfield movements in both the z and x directions are used as inputs in the proposed method, which can accept any generic greenfield displacement profiles resulting from the tunnelling process.

MODEL VALIDATION

Equivalent beam structure and perfect tie interface

Firstly, to display the reliability of the EL solution, the outcomes of the elastic TSI analyses performed by Haji et al. (2018a) were used for validation. Haji et al. (2018a) considered linear elastic isotropic solids in plane-strain conditions for both the soil and the structure as well as a perfect tie condition between the soil and the structure. The soil was modelled as an isotropic continuum with $E_s = 35$MPa and $\nu_s = 0.25$. For the tunnel, the diameter was $D = 4.65$m and the depth was $z_t = 13.6$m. The greenfield surface displacements used by Haji et al. (2018a) in the directions z and x at $V_{l,t} = 1.76\%$ were implemented. Two simple beam structures at the ground level (subscript bg) were modelled with a modulus of elasticity $E = 23$GPa, a Poisson's ratio $\nu = 0.15$, a transverse length $B = 60$m, and beam cross-sectional depths (i.e. beam heights) of $d_{bg} = 0.5, 3$m. Two tunnel-structure eccentricities were considered; the tunnel was located below the structure centre ($e/B = 0$) and the structure edge ($e/B = 0.5$), where e/B is the ratio between the eccentricity and the structure transverse length. To obtain EL solutions similar to plane-strain conditions, in the proposed EL solution the cross-sectional width (i.e. structure length in the tunnel direction) was set to $b_{bg} = 10$m.

The tunnelling-induced vertical and horizontal displacements of the beam mid-height from Haji et al. (2018a) and the proposed EL solution are shown in Figures 3 and 4 for the central and eccentric tunnel-structure configurations, respectively. For these figures, the sub-plots (a)-(b) display the displacements of the flexible structure ($d_{bg} = 0.5$m) whereas sub-plots (c)-(d) the movements for the stiff beam ($d_{bg} = 3$m). In particular, interaction analyses were performed considering three greenfield cases (distinguished by using varying colours): both vertical and horizontal movements, only greenfield vertical movements, and only horizontal displacements. For all the analysed scenarios, there is a good agreement between the EL solution (solid lines) and the benchmark data (markers). Importantly, for the stiff structures, the EL solution is able to predict the magnitude of both the vertical and horizontal displacements; therefore, the EL solution is suitable to model the response to tunnelling of foundations consisting of separated footings.

Equivalent beam structure and frictional interface

To validate the capability of the EP solution with a linear elastic soil model with secant values of soil stiffness, a comparison is carried out with centrifuge testing results from Farrell (2010) and Farrell et al. (2014), which model simple beams (STR) centrally located with respect to the tunnel of varying stiffness and weight. The axial and bending stiffness of the beams were specified to be representative of realistic foundation/superstructure systems.

Input soil movements were set equal to vertical and horizontal displacements measured during a centrifuge test of a greenfield tunnel excavation in uniform sand performed by Farrell (2010) (which was also published by Farrell et al. (2014) and Marshall et al. (2012)). This experiment was performed in plane-strain conditions by inducing a uniform distribution of tunnel volume loss in the model tunnel longitudinal direction. In particular, rather than implementing experimental raw data, fitted curves were used to limit the influence of the experimental noise in the measurements and obtain perfectly symmetric/asymmetric curves with respect to the tunnel centreline. The curve-fitting was performed as follows. At each $V_{l,t}^{exp}$ (experimental values at which a measurement was performed), vertical and horizontal movements at the ground surface were interpolated, respectively, with Equations (8) and (9), which are a modified Gaussian curve and a Gaussian curve based equation. As displayed by Farrell (2010), these empirical curves can achieve a good fit to movements measured during centrifuge testing of tunnelling in sands. In this paper, volume loss increments $\Delta V_{l,t} = 0.25\%$ were implemented up to the final value $V_{l,tmax} = 5\%$.

$$u_z = u_{z,max} \frac{n}{(n-1) + \exp\left[\alpha\,(x/i)^2\right]};\, n = e^{\alpha} \frac{2\alpha - 1}{2\alpha + 1} + 1 \tag{8}$$

$$u_x = u_{x,max} \frac{1.65x}{i_x} \exp\left[-\frac{x^2}{2i_x^2}\right] \tag{9}$$

In Equations (8) and (9), x is the horizontal spatial coordinate, $u_{z,max}$ is the maximum settlement, i is the horizontal distance of the settlement trough inflection point to the centreline, n is the shape function (if $n = 1$, $x^* = i$ then Equation (8) becomes the standard Gaussian curve), i_x is the horizontal offset of the maximum horizontal displacement $u_{x,max}$.

For the EL and EP solutions, Table 2 summarises the geotechnical model parameters (including Young's modulus, E_s, and Poisson's ratio, ν_s, of the soil) whereas Table 3 indicates the properties of the simple beams at the ground level (subscript bg) adopted for the validation (Young's modulus, E, beam length in the direction transverse to the tunnel, B, as well as cross-sectional depth, d_{dg}, and width, b_{dg}). A structural cross-section width $b_{dg} = 10$m was again adopted in the y direction to represent the nearly plane-strain conditions of the centrifuge tests.

Vertical displacements (u_z) of structures and sliders are shown in Figure 5 for the structures STR-1 and STR-4 at $V_{l,t} = 0.5, 2, 4\%$, which are tunnel ground losses ranging between low and extremely high values. Loads, q_z, representing the self-weight of the aluminium model structure used during the centrifuge tests were set to match the average contact pressures 3.2, 10.1, 20.3, and 40.5 kPa for STR-1, 2, 3, and 4, respectively. Solid lines are used for the tunnelling-induced structure displacement ($\mathbf{u}^{tun}$) obtained from the EP solutions, whereas dashed black lines are used for results of the EL analyses. Because no compressive limit force was implemented, tunnelling-induced plastic displacements of the sliders ($\mathbf{u}^{ip}$), represented with markers, are indicative of the gap between soil and foundation. Additionally, dotted lines are used to represent greenfield settlement troughs.

Results show that the EP solution could correctly model the main interaction mechanism resulting in the structure bending deformation both for the flexible structure STR-1 and the stiff model building STR-4. In particular, the EP solutions provided a reasonable prediction of [i] the decrease in building flexural distortions (i.e. curvature) and the deflection ratio (by definition, the distance between the settlement curve and the segment connecting two points of the curve) with bending stiffness, and, [ii] for the stiff structure the reduction in beam settlements with volume loss, which is the result of the gap formation. Load redistribution and gap formation are detailed as follows. The building self-weight causes the building to be distorted by tunnelling-induced movements. In the process, loads can be redistributed along the foundation and within the structure because of its stiffness. For example, the stiffness of the building causes the soil-structure contact pressure to be locally reduced or lost, causing an increase in contact pressures elsewhere.

On the other hand, the implemented EP solution does not account for the embedment of the rigid structure reported by Farrell et al. (2014), which is the consequence of soil plasticity. This embedment could have been partially captured in the EP solution by setting a compressive limit for the vertical springs (i.e. a finite value for $f_{i,up}$). However, a failure criterion for a given vertical slider should be defined by considering the forces applied to the soil at any other location in both the vertical and horizontal directions (i.e. by coupling the plastic sliders). The modelling of soil plasticity within two-stage analysis methods was achieved by Elkayam and Klar (2010) using macro-elements in the case of separated footings. However, to the authors' knowledge, further work is needed for raft foundations/strip footings. Additionally, although the soil plasticity contributes to tunnelling-induced structural settlements (Elkayam and Klar 2010), Elkayam (2013) displayed that two-stage solutions adopting elastic soil models (as in the proposed EL and EP solutions) provide a conservative estimation of tunnelling-induced deformations with respect to the elastoplastic soil models for a wide range of multi-storey structures.

With respect to the EL solution (i.e. fully elastic interaction analysis with perfect soil-structure bonding), Figure 5 suggests that the EL solution gives reasonable predictions of simple beam settlements for $V_{l,t} = 0.5 - 1\%$, whereas the gap formation should be taken into account (for this tunnelling scenario) at higher volume losses to avoid an overly conservative assessment. It should be noted that under the assumptions of the proposed EP solution, an infinitely heavy structure would settle according to the EL solution.

Horizontal displacements (u_x) of structures and sliders, with the latter modelling the slippage between foundation and soil, are shown in Figure 6. In the horizontal direction, the analysed structures (centrally located with respect to the tunnel) display negligible horizontal movements, which agrees with previous research showing that horizontal strains experienced by structures with continuous foundations may be negligible because of the high structural axial stiffness. In addition, the results show high slippage at the interface, and a different distribution for the structures STR-1 and STR-4. For the flexible beam with low weight (STR-1), the distribution of the slippage is approximately equal to greenfield movements and opposite in sign; for the deep beam with greater weight (STR-4), the plastic horizontal displacements are concentrated near the structure centre (between $x = \pm 8$m). The latter distribution is a direct consequence of Equation (7). Due to load redistribution and gap formation, the soil is completely unloaded in the centre of the structure above the tunnel (thus, the limit horizontal forces are decreased to zero), whereas the magnitude of limit frictional forces is increased at the structure edges.

Results confirmed that the EP prediction of the structural deformations is reasonably good for typical ratios of building weight and stiffness. However, judgement is necessary when applying the EL and EP methods to fully-flexible structures with extremely large vertical service loads that can settle and deform more than the greenfield conditions (Giardina et al. 2015). In these cases (which are not frequent in practice because stiffness often increases with building weight) there is a potential underestimation of the magnitude of structural deformations with the proposed solutions.

FOUNDATION AND SUPERSTRUCTURE DISPLACEMENTS

Simple beams with varying foundation scheme

In this section, simple beams with either a continuous foundation or a foundation comprising separated footings equally spaced (see cases STR and BE in Figure 2) as well as varying building load, q_z, were investigated. For structures STR the same structural properties were assumed as in the previous section (see Table 3), except that a structural cross-section of unit width in the y direction was adopted ($b_{bg} = 1$m). The BE structure was implemented by [i] modelling the footings with beam elements and [ii] adding the condensed contribution of the superstructure to the central nodes of the foundation elements. The properties of the implemented BE structures are detailed in Table 5. The characteristics (E, B, d) of the beams BE are identical to the structures STR; a 5-footing foundation configuration (subscript f) was modelled with footing width (perpendicular to the tunnel) of $B_f = 3$m, cross-sectional footing width (parallel to the tunnel) of $b_f = 1$m, footing depth of $d_f = 3$m, and footing spacing of $l = 7.5$m. BE structures are not meant to represent a realistic building, but are used to investigate the effect of the continuity of the foundation alone on the structural response, before evaluating frame-type structures on isolated footings. Four different uniformly distributed vertical loads were used, as detailed in Table 4 (however, results for q_{30} are only provided in the supplemental data). The geotechnical parameters described by Table 2 and the input greenfield ground movements from centrifuge test results (Farrell (2010)) were adopted in subsequent analyses; the soil stiffness was estimated for $V_{l,t} = 4\%$ by Ritter (2017). A unique tunnelling scenario was considered in this section because the main aim is the study of the structural configuration effects on TSI.

Figure 7 compares the vertical and horizontal displacements of STR-2/4, and BE-2/4 for a tunnel located centrally with respect to the structure. The layout (line style and colours) of this figure is consistent with previous plots, but results were limited to $V_{l,t} = 2\%$. For comparison, smoothed centrifuge greenfield ground movements are again plotted with dotted lines. Results illustrate that, for the given structural configuration (i.e. simple beams) and foundation elements being affected by similar distributions of greenfield movements, the influence of the foundation configuration on the TSI mechanism was secondary. When high structure loads decrease the gap formation, [i] the structure shows a more flexible behaviour and [ii] it undergoes greater settlements. Also note the effects of the structure load q_z on the slippage level and that the gap starts to affect the response of both stiff and semi-flexible structures with a low weight (q_{10}) from medium volume losses ($V_{l,t} = 2\%$). However, additional analyses performed for 3-footing foundations displayed that the tunnel-structure interaction of structures STR and BE could be different because of a reduction in the contact area between the foundation and the soil as well as potential of a different distribution of greenfield movements.

To analyse the impact of the tunnel-structure eccentricity, simple beams on continuous foundations (STR) are subjected to the ground movements resulting from three different relative eccentricities $e/B = 0$, 0.25 and 0.5 (where e is the horizontal distance between the tunnel centreline and the structure centre). Supplemental data reported in Figure S1 provides vertical and horizontal displacements of the structures STR-2 and STR-4. For the analysed cases, the increase in the superstructure EI resulted in a fully sagging or hogging deformation of the stiff structures despite the greenfield profiles have both sagging and hogging parts. With respect to the sliders, results indicate that the gap magnitude decreased with the tunnel horizontal offset e and (when induced) tended to concentrate directly above the tunnel, while secondary uplift at the edges of stiff structures may also occur. On the other hand, horizontal structural strains were negligible for both central and eccentric tunnels, whereas tunnelling results in a minor shift of the structure towards the tunnel centreline that is greater for $e/B = 0.5$ than $e/B = 0.25$.

Frames and bridges on separated footings

To investigate frame buildings and bridges on separated footings, the framed structural schemes FR, FRB and BR and the distribution of vertical structural loads illustrated in Figure 2 were modelled. Only single-storey schemes are considered in this section. Structural characteristics are summarised in Table 1, where subscripts c and b are used for the superstructure columns and beams, respectively. To allow for the comparison with results in previous sections, structures FR/FRB/BR in this section were obtained by including deformable columns between the footings and the simple beam of the structures BE with a 5-footing foundation. Two type of cross-sections, identical to the simple beams of BE-2 and BE-4, were selected for the columns (labelled with the suffix c2 and c4, respectively). Frame buildings (labelled FR and FRB) and bridges (labelled BR) have a storey height $h = 3$ and 9m, respectively. Finally, with respect to structures FR, frames FRB have an additional floor slab integrated with the footings, which was modelled with a flexible ground level beam (subscript bg in Table 1) connecting the centres of the footings.

The response of single-storey structures FR, FRB and BR centrally located with respect to the tunnel ($e/B = 0$) is illustrated by Figures 8 and 9. In Figure 8, vertical and horizontal foundation displacements are plotted for varying column stiffness (c2 and c4) for the cases of relatively flexible and stiff beams (FR/FRB/BR-2 and FR/FRB/BR-4) at $V_{l,t} = 2‰$. On the other hand, Figure 9 illustrates the deformed shape of the framed superstructures FR-4c2, FR-4c4, FRB-4c4 and BR-4c4 corresponding to the foundation movements shown in Figures 8(e)-(h) and (o)-(r) for $q_z = 100\text{kN/m}$ (dark marker). Note that the displacements of these superstructure were computed imposing the solution displacement $\mathbf{u}_{su}$ at the superstructure base.

As can be seen from Figures 8 and 9, complex rotation-translation displacements of the footings occurred. This is due to the coupling between the vertical and horizontal DOFs of the base nodes of frames. Figure 10 illustrates this coupling. Figure 10(a) shows that if the base nodes of the frame FR-4c2 are displaced vertically as in Figure 9(c) while releasing the horizontal and rotational DOFs, the deflection of the beam results in the rotation of the column heads as well as the horizontal translation of the column bases. On the other hand, in Figure 10(b), the superstructure was displaced by the horizontal foundation movements reported in Figure 9(c) while releasing the remaining DOFs; the resulting differential horizontal displacements induce the deflection of the columns, whereas the vertical displacements of the beams are minor due to the low column-beam bending stiffness ratio of FR-4c2 and the counteracting effect of positive and negative horizontal displacements of the foundation.

In the following, the term 'local greenfield rotation' is used to describe the average first derivative of the greenfield settlement curve at the location of a given footing. In Figures 8(a)-(h), foundation settlements (u_z) illustrate the following: [i] the rotation of the footings may be opposite to the local greenfield rotation; [ii] column stiffening effects can reduce the relative deflection of the structure as well as decrease the difference between footing and local greenfield rotations; [iii] for separated footings (structures FR and BR) supporting columns with the same cross-section, there is a decrease in the structure relative deflection with the column height, as shown by the deflection response of BRc4 being lower than that of FRc4 (compare Figures 8(b)-(d) and (f)-(h) as well as Figures 9(a) and (d))); [iv] the presence of the floor slab at the ground level (through its axial stiffness) in structures FRB tends to decrease the frame relative deflection (compare Figures 8(f) and (g) as well as Figures 9(a) and (b))); [v] there is an influence of the superstructure load condition on the rotation-translation displacement mechanism of the footings (i.e. the reduction in the load can affect foundation settlements and rotations). Interestingly, the mechanisms described in points [iii] and [iv] have not been detailed by previous research.

Next, foundation horizontal displacements are considered. From Figures 8(i)-(r), it can be seen that differential horizontal movements of the foundation are small for footings integrated with a structural slab (FRB), whereas separated footings with no ground level connection (FR, BR) experience a complex distribution of footing horizontal displacements (u_x), although their magnitudes are lower than vertical settlement values. Horizontal strains resulting from the differential horizontal displacements are remarkable, as discussed in a subsequent section.

The complex behaviour of the soil-structure system is partially due to the coupled response of the frame in x and z (as described by Figure 10) and it is dependent on both column stiffness and column height. In particular, data was analysed with respect to the stiffness parameters EI_c/h and EI_b/l, where EI_c and EI_b are the bending stiffness of the column and the beam, respectively. Firstly, results for low values of soil-foundation slippage ($q_z > q_{30}$) are analysed. Figures 8(i), (n) and (o) indicate that columns with low EI_c/h are associated with a distribution of u_x that agrees in shape with the greenfield values, whereas the rotation of the footings is opposite in sign to local greenfield rotations (see Figures 8(a), (d) and (e)). For pile foundations, a similar rotation-translation interaction mechanism was described for frame buildings by Franza et al. (2017). On the other hand, Figures 8(l)-(p) and (n)-(r) display that, for framed superstructure with high EI_c/h, the increase in the stiffness of the beam EI_b/l induced displacements of the footings outwards with respect to the tunnel centreline. Interestingly, framed superstructures with high EI_c/h and EI_b/l (Figures 8(p) and (q)) are associated with a distribution of footing rotations shaped as local greenfield rotations (see Figures 8(f) and (g)); this is probably due to the beam deflecting with a constant curvature and the columns rotating as a rigid body, as displayed in Figure 9(a). Secondly, note that the decrease in the structure vertical load results in slippage (as expected due to decreased limit horizontal frictional force) that induced outwards movements of the foundation as well as a decrease in the difference between footing and greenfield rotations (for instance, in Figures 8(b) and (l)).

Regarding observation [iii], the reduction in deflection (i.e. angular distortion) of the beam caused by longer columns (i.e. more flexible columns) was unexpected. This occurred because for structures without the ground level slab, the lack of footing horizontal constraint resulted in the horizontal reaction forces of the soil at the column bases being approximately constant with variation in the column height (as discussed in the next sections). Due to an increase in the lever arm (given by the column height) between these horizontal reaction forces at the footings and the first-storey beam, the bending movements transmitted by the column head to the first-storey beam increased, reducing the beam deflection. Note that observation [iii] is contrary to Goh and Mair (2014), which indicates that for multi-storey frames the stiffening effect of the columns decreases with storey height h. However, the difference is a consequence of the assumption of Goh and Mair (2014) that horizontal displacements at the column mid-height do not occur (which should be a valid assumption for multi-storey frames). Point [v], which indicates that the flexural response due to tunnelling beneath frames depends also on the level of horizontal constraint of its structural elements, is relevant. If column bases are horizontally fixed by the ground level slab, the beam-column head rotation due to beam deflection resulted in greater horizontal forces (given by the slab) at the column bases and greater bending moments at the first-storey beam; consequently, floor slabs significantly increased the column stiffening effects and, thus, the overall flexural stiffness of the frame with respect to settlement troughs.

Finally, it has to be noted that this study focused on single-storey frames, while specifically evaluating the influence of the number of stories on the tunnel-soil-structure interaction is beyond the objectives of the paper. However, the conclusions of this study deal with the movements of the foundation, which are highly dependent on the foundation scheme, and would similarly apply to both single and multi-storey frames. More detailed conclusions regarding the response to tunnelling of multi-storey frames requires further investigation (Haji et al. 2018b; Franza and DeJong 2018).

SUPERSTRUCTURE LOAD TRANSFER MECHANISMS

In recent years, a lot of attention has been focused on excavation-induced displacements and strains of structures. However, the soil-structure interaction also involves redistribution of pressures beneath the foundation (Boldini et al. 2018; Farrell et al. 2014; Giardina et al. 2017), which has been referred to as a tunnelling-induced load transfer mechanism ('LTM'). Note that, although complete loss of contact between the foundation and the soil may be unlikely under certain scenarios (e.g. wide settlement troughs, heavy structures, low volume losses), an LTM always occurs when the structure does not follow the greenfield ground movement. Therefore, quantifying the load transfer can provide further understanding of the soil-structure interaction, and could be used to evaluate in frame structures potential damage, which is related to the superstructure capacity to withstand post-tunnelling distribution of inner forces (depending on LTMs).

To study LTMs resulting from tunnel volume loss, reactions of the superstructure, $\mathbf{R}$, are plotted in Figure 11 against $V_{l,t}$ for varying load conditions. These reactions (axial (vertical) forces, N, shear (horizontal) forces, V, and bending moments, M) are the forces/moments applied by the superstructure base to the foundation due to tunnelling-induced movements; therefore, $\mathbf{R} = -\mathbf{K}_{su}\mathbf{u}^{tun}$. In particular, the influence of the structural configuration is assessed by comparing the forces and bending moments associated with simple beams (BE-4) and framed structures on separated footings (FR-4c2/4 and BR4c4) for $e/B = 0$. For instance, considering the sign convention shown in Figure 2, a negative axial reaction indicates vertical unloading of foundation elements. To distinguish between reaction locations, footings are named Foot1-Foot5, starting from an offset x of -15m through to $+15$m. Given the symmetry with respect to the tunnel centreline, only results corresponding to Foot1, 2, and 3 are displayed in this figure.

As shown in Figure 11, the LTMs tend to follow non-linear trends for the considered structures with a stiff beam. This was due to the plastic thresholds of the sliders (i.e. gap formation and slippage) being fully reached. Furthermore, the greater the weight of the structure, the higher the transferred loads and the greater the volume loss at which there was a transition from a linear to a non-linear problem. It should be noted that the footings directly above the tunnel are unloaded, but these vertical reactions are not necessarily transferred towards the immediately adjacent footings. Also note that plastic deformation of the soil, which would cause nonlinear behaviour at lower levels of volume loss, is not considered in the adopted solutions.

The reactions of simple beams and framed structures are then compared. Based on the data shown in the left column of Figure 11, the variation of vertical reaction forces with volume loss ($N - V_{l,t}$) is similar for all structures, despite a greater increase in the loading of the external footings Foot1/Foot5 of BR-4c4. It is also interesting to compare the qualitative distribution of shear reaction forces, V (central column of Figure 11). The trends corresponding to the intermediate Foot2/Foot4 (dashed lines) are similar between simple beams and framed structures, whereas there is a difference in the reactions at Foot1/Foot5 (dotted lines), at which the greenfield horizontal displacements u_x are close to zero. For simple beams, V at the superstructure edges were negligible because there is little greenfield movement there; for framed structures, horizontal reaction forces at Foot1/Foot5 are induced by greater differential horizontal movements between footings, which were partially due to the coupling between vertical and horizontal DOFs of the superstructure base. Figures 11(e), (h), and (m) demonstrate the influence of frame characteristics. The increase in the column flexibility (associated with the decrease of the bending stiffness, FR-4c2, or the increase in the column height, BR-4c4, results in a lowering of V at Foot2/Foot4 for heavy structures (q_z = 100kN/m), whereas, at the same location, there is a slight variation in V values for lower structural loads (q_z = 30kN/m). Finally, the bending movements shown in the right column of Figure 11 display a correlation between the trends of M and the characteristics of the columns. BE-4 and FR-4c4 display similar M curves that are characterised by Foot1/Foot5 and Foot2/Foot4 transmitting opposing moments to the superstructure. On the other hand, despite the bending flexibility of the columns, BR-4c4 and FR-4c2 are associated with reaction moments at the intermediate Foot2/Foot4 that are greater than for BE-4 and FR-4c4, whereas bending moments are small at the external Foot1/Foot5 and agree in sign with bending moments applied to Foot2/Foot4.

The effects of tunnel normalised eccentricity were also investigated by analysing axial reactions and bending moments of simple beams on separated footings (BE-2/4) for $e/B = 0, 0.25, 0.5$; these supplemental data are provided in Figure S2. This dataset shows that the LTM is dependent on e/B as well as and the reaction distribution, for the given structural configuration BE, can qualitatively vary with the structural stiffness.

DEFORMATION PARAMETERS

Tunnelling-induced structural deformations are commonly assessed through the sagging and hogging deflection ratio (DR_{sag} and DR_{hog}) as well as tensile and contractive horizontal strains ($\varepsilon_{h,t}$ and $\varepsilon_{h,c}$) defined with respect of the foundation displacements at the surface level. To account for the foundation scheme, settlements of the footing central nodes were curve-fitted, then the DR was calculated as the distance between this curve and the segment connecting two of its points. ε_h were computed between the locations of the separated footings with the finite difference method considering the differential horizontal displacements and the distance between consecutive footings.

This approach based on the deformation parameters DR and ε_h, which was developed for continuous structures that can be more realistically simplified to beam structures, has limitations. In the case of framed structures on separated footings, as displayed by Figure 9, differential horizontal movements (measured in terms of ε_h) primarily result in the [i] deflection and [ii] rotation of the columns rather than [iii] axial strain of the beam. Only the contributions [i] and [iii] are damage-related parameters associated with structural deformations. However, in this study, ε_h are studied without distinguishing between these three mechanisms. Additionally, framed structure deformations also depend on the footing rotations, which are not accounted for by DR and ε_h. Therefore, although in this section DR and ε_h are quantified for the analysed cases, there is no available analytical framework for framed buildings that can use these values to compute a representative strain level.

Maximum deformation parameters (DR; ε_h) associated with the structures BE, FRc4, FRBc4, and BR on separated footings are plotted in Figure 12 against $V_{l,t}$ and for $e/B = 0$ (supplemental data for varying e/B and column stiffness is provided in Figure S3). Included in these figures are the maximum deformation parameters associated with greenfield movement profiles. DR_{sag} and $\varepsilon_{h,c}$ have negative values; DR_{hog} and $\varepsilon_{h,t}$ are defined positive. Therefore, it is possible to give the results either in sagging and hogging regions or for tensile and compressive strains within a unique sub-plot. To highlight the influence of the load condition, light and dark colours are used; to distinguish between the structural schemes, the line style is varied.

Figures 12(a)-(b) show that the difference in DR between BE and FR/FRB/BR structures, due to the stiffening effects of the columns, highly depended on the structural load condition, q_z, and tunnel volume loss, $V_{l,t}$. Furthermore, DR_{hog} and DR_{sag} of simple beams BE are generally higher than for framed structures FR/FRB/BR because of the column stiffening effect. This difference in DR between BE-4 and FR/FRB/BR-4 is greater than zero starting at low volume losses (i.e. $V_{l,t} = 0.5\%$), whereas for beams with low stiffness (BE-2 and FR/FRB/BR-2) it is significant only for $V_{l,t} > 1.0 - 1.5\%$. In addition, for semi-flexible framed superstructures FR/FRB/BR-2, there is a notable reduction of DR with respect to BE-2 at $V_{l,t} > 3 - 4\%$ (see sub-plot (a)). Next, data in sub-plot (b) confirm the reduction of the structure deflection with the addition of the floor slab (compare structures FR and FRB) or the increase in the column height for separated footings (see FRc4 and BR). Finally, although greenfield settlements were associated with both sagging and hogging deflection ratios, for stiff structures FR/FRB/BR-4 with low tunnel-structure eccentricity the structures display a fully sagging deformation.

Figures 12(c)-(d) display that ε_h values may be as large as the DR magnitude in the case of frames FR and BR, whereas horizontal strains are approximately zero for simple beam structures (BE) and framed structures with either a ground level slab or a footing connection beam (FRB). From the figures, it can be seen that: [i] increased with column height (e.g. values are lower for FRc4 than BRc4), whereas [ii] the correlation between ε_h and the load condition q_z is complex and affected by both the superstructure type and the tunnel-structure eccentricity (note that the reduction in q_z either increased or decreased ε_h depending on the considered case). The increase in ε_h with the reduction in q_z is probably due to the effects of soil-foundation slippage that sometimes led to remarkable horizontal movements of the foundation, as shown by Figure 8 (this is opposed to the gap formation that decreases structural settlements). In particular, during TSI analyses for eccentric structures provided within the supplemental data, slippage could result in ε_h greater than greenfield values and could induce a sharp rise in horizontal strains with tunnel volume loss.

Because greenfield flexural deformation parameters were mostly greater than the values obtained from TSI analyses, it could be argued that imposing greenfield movements at the structure foundation is a conservative approach for frame buildings and bridges. However, applying greenfield movements is a misleading approach. As shown in Figure 8, u_x curves of framed structures may be qualitatively different from the greenfield displacement profiles; additionally, footing and greenfield local rotations may differ. A soil-structure interaction analysis is needed to capture these effects.

CONCLUSIONS

This paper illustrates the capability of two-stage elastoplastic solutions for tunnel-structure interaction, which can be useful in the preliminary assessment stages for new tunnels. Results provide insights into tunnelling-induced deformation and load redistribution mechanisms of surface structures, emphasising the role played by the particular framed configuration and foundation scheme of linear elastic structures. The main conclusions of this work are:

- For superstructures that can be modelled by an equivalent simple beam at the ground level (e.g. bearing wall structures), the response of the structure to tunnelling was not qualitatively affected by the foundation scheme (continuous foundation or separated footings): bending deformations were predominately induced while horizontal strains are minor.
- For framed structures on separated footings, there was evidence of a complex rotation-translation response of the foundation that depended on the superstructure characteristics,

load condition, and the presence of a horizontal structural element connecting the footings (its axial stiffness can affect the flexural response to tunnelling of framed structures). In particular, separated footings of framed structures without horizontal connection slab displayed remarkable differential movements in the horizontal direction.

- The displacements of the base of framed superstructures were shown to be coupled in the vertical and horizontal directions (e.g. vertical frame deflections can result in differential horizontal displacements between columns at the ground level). Therefore, analytical frameworks that completely decouple axial and bending behaviours of frames on separated footings would lead to erroneous estimates of tunnelling-induced deformations.
- For frame buildings and bridges on separated footings, the shape of tunnelling-induced foundation movements differed from the greenfield distributions. In these scenarios, uncoupled analyses that force the structure base/foundation to follow greenfield settlement troughs and damage assessment methods developed for simple beams lack a physical basis.
- Evaluating load redistribution provided a useful measure to compare soil-structure interaction for the variety of structures considered. Load redistribution depended on both structure configuration and load condition.
- Gap formation and slippage beneath the foundation were modelled. Tunnelling-induced flexural deformations of structures could be overestimated if gap formation is not allowed (in particular, for semi-flexible structures with modest loads), whereas slippage can result in significant differential horizontal displacements between separated footings of framed structures. In addition, results suggested that gap formation and slippage could induce non-linear trends of load redistribution and structure deformation with tunnel volume loss.

ACKNOWLEDGEMENTS

This work was supported by the Engineering and Physical Sciences Research Council (EPSRC) [EP/N509620/1]. The research materials supporting this publication can be accessed at https://doi.org/10.17863/CAM.25766.

SUPPLEMENTAL DATA

Figures S1-S3 are available online in the ASCE Library [link will be added].

REFERENCES

Basmaji, B., Deck, O., and Al Heib, M. (2017). "Analytical model to predict building deflections induced by ground movements." *Eur. J. Environ. Civ. Eng.*, 1–23.

Bilotta, E., Paolillo, A., Russo, G., and Aversa, S. (2017). "Displacements induced by tunnelling under a historical building." *Tunn. Undergr. Sp. Technol.*, 61, 221–232.

Boldini, D., Losacco, N., Bertolin, S., and Amorosi, A. (2018). "Finite Element modelling of tunnelling-induced displacements on framed structures." *Tunn. Undergr. Sp. Technol.*, 80, 222–231.

Deck, O. and Singh, A. (2012). "Analytical model for the prediction of building deflections induced by ground movements." *Int. J. Numer. Anal. Methods Geomech.*, 36(1), 62–84.

Elkayam, I. (2013). "Tunneling induced ground displacements and their effects on structures." *Ph.D. Thesis, Tech. - Isr. Inst. Technol.*

Elkayam, I. and Klar, A. (2010). "Nonlinear Analysis of Tunneling Effects on Buildings Using Macro-Elements." *GeoFlorida 2010*, Vol. 199 GSP, Orlando, Florida, United States, American Society of Civil Engineers, 2301–2310.

Fargnoli, V., Gragnano, C. G., Boldini, D., and Amorosi, A. (2015). "3D numerical modelling of soil–structure interaction during EPB tunnelling." *Géotechnique*, 65(1), 23–37.

Farrell, R. (2010). "Tunnelling in sands and the response of buildings." *Ph.D. Thesis, Cambridge Univ.*

Farrell, R., Mair, R., Sciotti, A., and Pigorini, A. (2014). "Building response to tunnelling." *Soils Found.*, 54(3), 269–279.

Franza, A. and DeJong, M. J. (2017). "A simple method to evaluate the response of structures with continuous or separated footings to tunnelling-induced movements." *Proceeding Congr. Numer. Methods Eng. 2017*, I. Arias, J. M. Blanco, S. Clain, P. Flores, P. Lourenço, J. J. Ródenas, and M. Tur, eds., Valencia, Spain, 919–931.

Franza, A. and DeJong, M. J. (2018). “Discussion of “A cantilever approach to estimate bending stiffness of buildings affected by tunnelling” by Twana Kamal Haji, Alec M. Marshall, and Walid Tizani.” *Tunn. Undergr. Sp. Technol.*, 77, 314–315.

Franza, A., Marshall, A. M., Haji, T., Abdelatif, A. O., Carbonari, S., and Morici, M. (2017). “A simplified elastic analysis of tunnel-piled structure interaction.” *Tunn. Undergr. Sp. Technol.*, 61, 104–121.

Franzius, J. N., Potts, D. M., and Burland, J. B. (2006). “The response of surface structures to tunnel construction.” *Proc. ICE - Geotech. Eng.*, 159(1), 3–17.

Fu, J., Yu, Z., Wang, S., and Yang, J. (2018). “Numerical analysis of framed building response to tunnelling induced ground movements.” *Eng. Struct.*, 158, 43–66.

Giardina, G., DeJong, M. J., and Mair, R. J. (2015). “Interaction between surface structures and tunnelling in sand: Centrifuge and computational modelling.” *Tunn. Undergr. Sp. Technol.*, 50, 465–478.

Giardina, G., Ritter, S., DeJong, M., and Mair, R. (2017). “The role of building position on the response of buildings to tunnelling subsidence: numerical modelling.” *Proceeding 9th Int. Symp. Geothecnical Asp. Undergr. Constr. Soft Gr. (IS-São Paulo 2017)*, São Paulo, Brazil.

Goh, K. H. and Mair, R. J. (2014). “Response of framed buildings to excavation-induced movements.” *Soils Found.*, 54(3), 250–268.

Haji, T. K., Marshall, A. M., and Franza, A. (2018a). “Mixed empirical-numerical method for investigating tunnelling effects on structures.” *Tunn. Undergr. Sp. Technol.*, 73, 92–104.

Haji, T. K., Marshall, A. M., and Tizani, W. (2018b). “A cantilever approach to estimate bending stiffness of buildings affected by tunnelling.” *Tunn. Undergr. Sp. Technol.*, 71, 47–61.

Kitiyodom, P., Matsumoto, T., and Kawaguchi, K. (2005). “A simplified analysis method for piled raft foundations subjected to ground movements induced by tunnelling.” *Int. J. Numer. Anal. Methods Geomech.*, 29(15), 1485–1507.

Klar, A., Vorster, T. E., Soga, K., and Mair, R. J. (2007). “Elastoplastic solution for soil-pipe-tunnel interaction.” *J. Geotech. Geoenvironmental Eng.*, 133(7), 782–792.

Klar, A., Vorster, T. E. B., Soga, K., and Mair, R. J. (2005). "Soil-pipe interaction due to tunnelling : comparison between Winkler and elastic continuum solutions." *Géotechnique*, 55(6), 461–466.

Leung, Y. F., Klar, A., and Soga, K. (2010). "Theoretical Study on Pile Length Optimization of Pile Groups and Piled Rafts." *J. Geotech. Geoenvironmental Eng.*, 136(2), 319–330.

Losacco, N., Burghignoli, A., and Callisto, L. (2014). "Uncoupled evaluation of the structural damage induced by tunnelling." *Géotechnique*, 64(8), 646–656.

Mair, R. (2013). "Tunnelling and deep excavations: ground movements and their effects." *Proc. 15th Eur. Conf. Soil Mech. Geotech. Eng. - Geotech. Hard Soils - Weak Rocks (Part 4)*, A. Anagnostopoulos, M. Pachakis, and C. Tsatsanifos, eds., Amsterdam, the Netherlands, IOS Press, 39 – 70.

Mair, R. J., Taylor, R. N., and Burland, J. B. (1996). "Prediction of ground movements and assessment of risk of building damage due to bored tunnelling." *Proc. Int. Symp. Geotech. Asp. Undergr. Constr. Soft Gr.*, R. J. Mair and R. N. Taylor, eds., London, United Kingdom, Balkema, Rotterdam, 713–718.

Marshall, A. M., Farrell, R., Klar, A., and Mair, R. (2012). "Tunnels in sands: the effect of size, depth and volume loss on greenfield displacements." *Géotechnique*, 62(5), 385–399.

Pickhaver, J., Burd, H., and Houlsby, G. (2010). "An equivalent beam method to model masonry buildings in 3D finite element analysis." *Comput. Struct.*, 88(19), 1049–1063.

Potts, D. M. and Addenbrooke, T. I. (1997). "A structure's influence on tunnelling-induced ground movements." *Proc. ICE - Geotech. Eng.*, 125(2), 109–125.

Ritter, S. (2017). "Experiments in tunnel-soil-structure interaction." *Ph.D. thesis, Univ. Cambridge*.

Ritter, S., Giardina, G., DeJong, M. J., and Mair, R. J. (2017). "Centrifuge modelling of building response to tunnel excavation." *Int. J. Phys. Model. Geotech.*

Vaziri, H., Simpson, B., Pappin, J. W., and Simpson, L. (1982). "Integrated forms of Mindlin's equations." *Géotechnique*, 32(3), 275–278.

Vesic, A. B. (1961). "Bending of beams resting on isotropic elastic solid." *J. Eng. Mech. Div.*, 87(EM2, Part 1), 35–53.

List of Tables

TABLE 1. Framed structure properties.

Label	Type (# storeys)	E (GPa)	B (m)	h (m)	B_f (m)	l (m)	d_b (m)	d_c (m)	d_{bg} (m)	d_f
FR-2c2	Frame (1)	70	30	3	3	7.5	0.375	0.375	–	3
FR-2c4	Frame (1)	70	30	3	3	7.5	0.375	1.5	–	3
FR-4c2	Frame (1)	70	30	3	3	7.5	1.5	0.375	–	3
FR-4c4	Frame (1)	70	30	3	3	7.5	1.5	1.5	–	3
FRB-2c2	Frame (1)	70	30	3	3	7.5	0.375	0.375	0.12	3
FRB-2c4	Frame (1)	70	30	3	3	7.5	0.375	1.5	0.12	3
FRB-4c2	Frame (1)	70	30	3	3	7.5	1.5	0.375	0.12	3
FRB-4c4	Frame (1)	70	30	3	3	7.5	1.5	1.5	0.12	3
BR-2c4	Bridge (1)	70	30	9	3	7.5	0.375	1.5	–	3
BR-4c4	Bridge (1)	70	30	9	3	7.5	1.5	1.5	–	3

$b_b = b_c = b_{bg} = b_f = 1$m

TABLE 2. Geotechnical model parameters.

Tunnel			Soil		
z_t	(m)	11.25	E_s	(MPa)	25
R	(m)	3.075	ν_s	(−)	0.25
$V_{l,tmax}$	(%)	5	μ	(−)	$\tan(30°)$
$\Delta V_{l,t}$	(%)	0.25			

TABLE 3. Simple beams properties.

Label	Type	E (GPa)	B (m)	d_{bg} (m)
STR-1	Beam	70	30	0.12
STR-2	Beam	70	30	0.375
STR-3	Beam	70	30	0.75
STR-4	Beam	70	30	1.5

TABLE 4. Loads for parametric study of weight influence.

	q_z (kN/m)
q_{10}	10
q_{30}	30
q_{50}	50
q_{100}	100

TABLE 5. Simple beams on separated footings.

Label	Type	E (GPa)	B (m)	B_f (m)	l (m)	d_{bg} (m)	d_f (m)
BE-2	Beam	70	30	3	7.5	0.375	3
BE-4	Beam	70	30	3	7.5	1.5	3
							$b_{bg} = b_f = 1$m

List of Figures

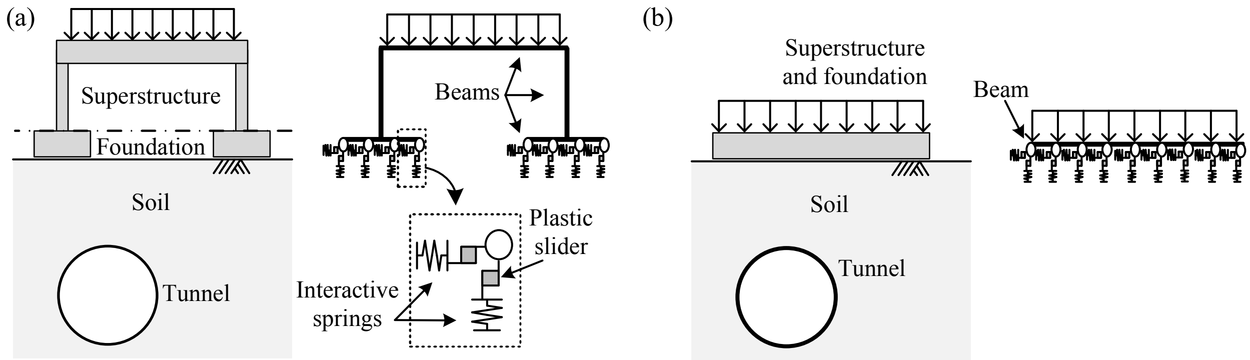

Fig. 1. Sketches of the building configuration and representation of the mechanical model for (a) the frame superstructure model and (b) the equivalent beam model.

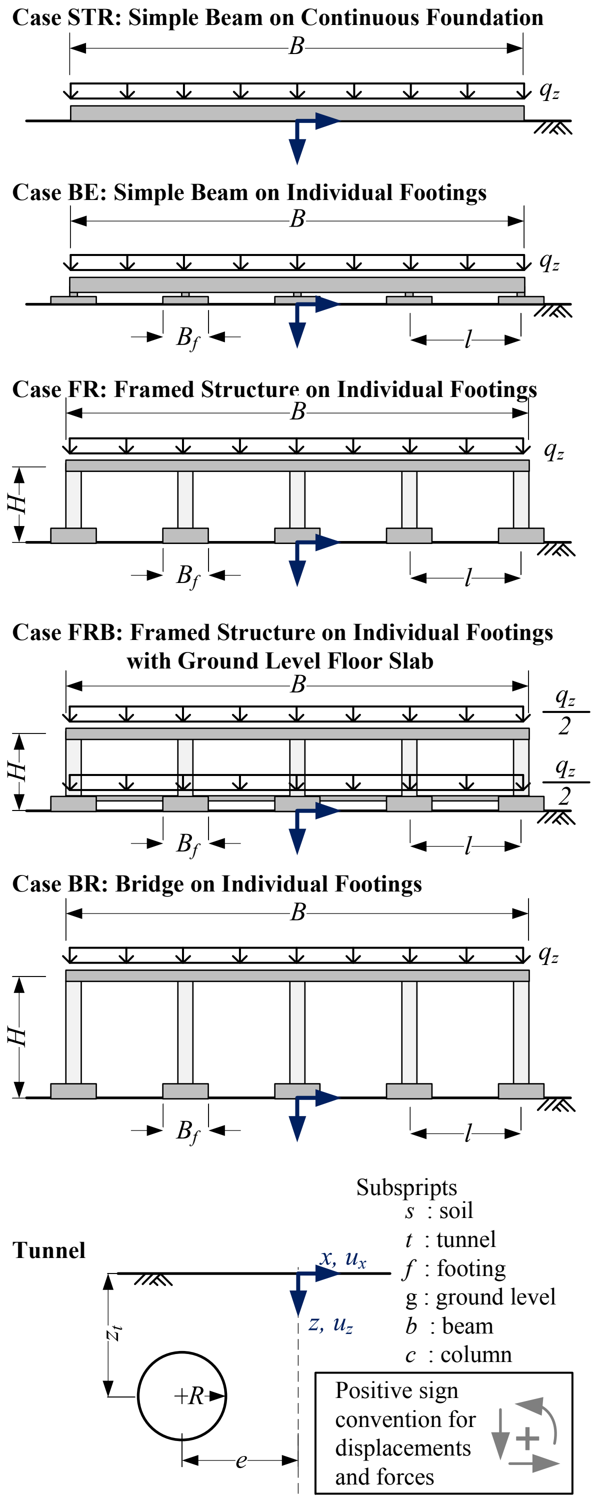

Fig. 2. Studied structural configurations.

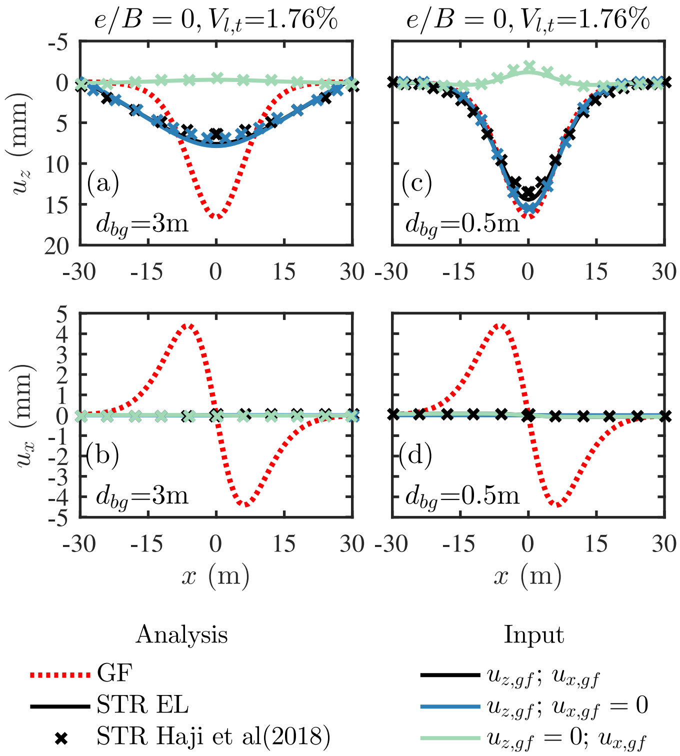

Fig. 3. Comparison of the elastic solution EL with ABAQUS elastic modelling: central structure with $e/B = 0$.

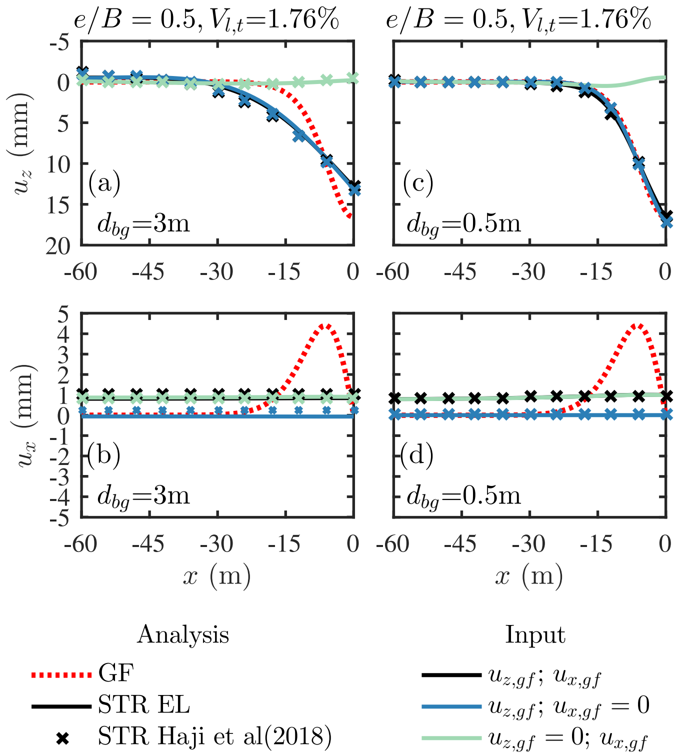

Fig. 4. Comparison of the elastic solution EL with ABAQUS elastic modelling: eccentric structure with $e/B = 0.5$.

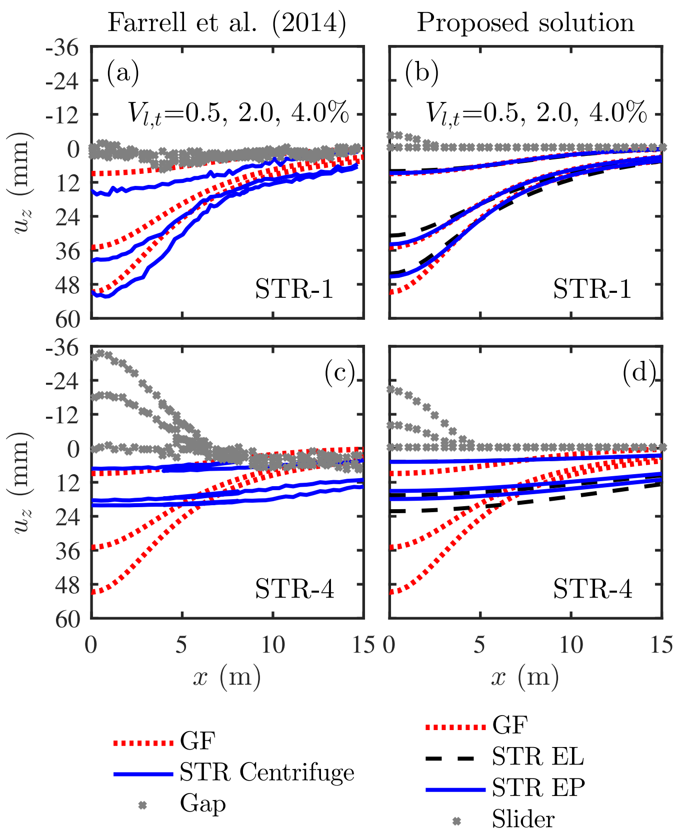

Fig. 5. Settlements and gap: (a) and (c) cetrifuge data (Farrell et al. 2014), (b) and (d) results from the proposed EL and EP solutions.

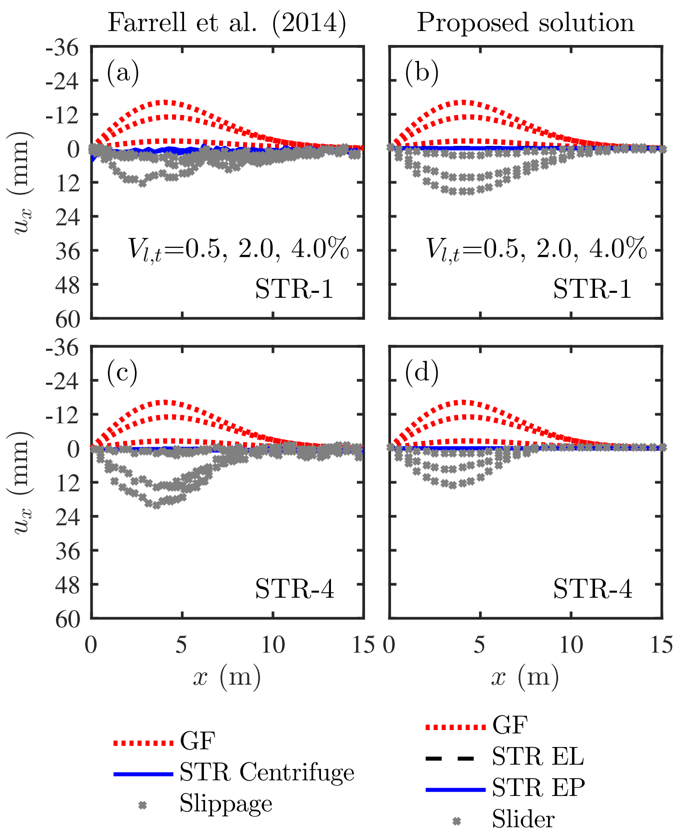

Fig. 6. Horizontal displacement and slippage: (a) and (c) cetrifuge data (Farrell et al. 2014), (b) and (d) results from the proposed EL and EP solutions.

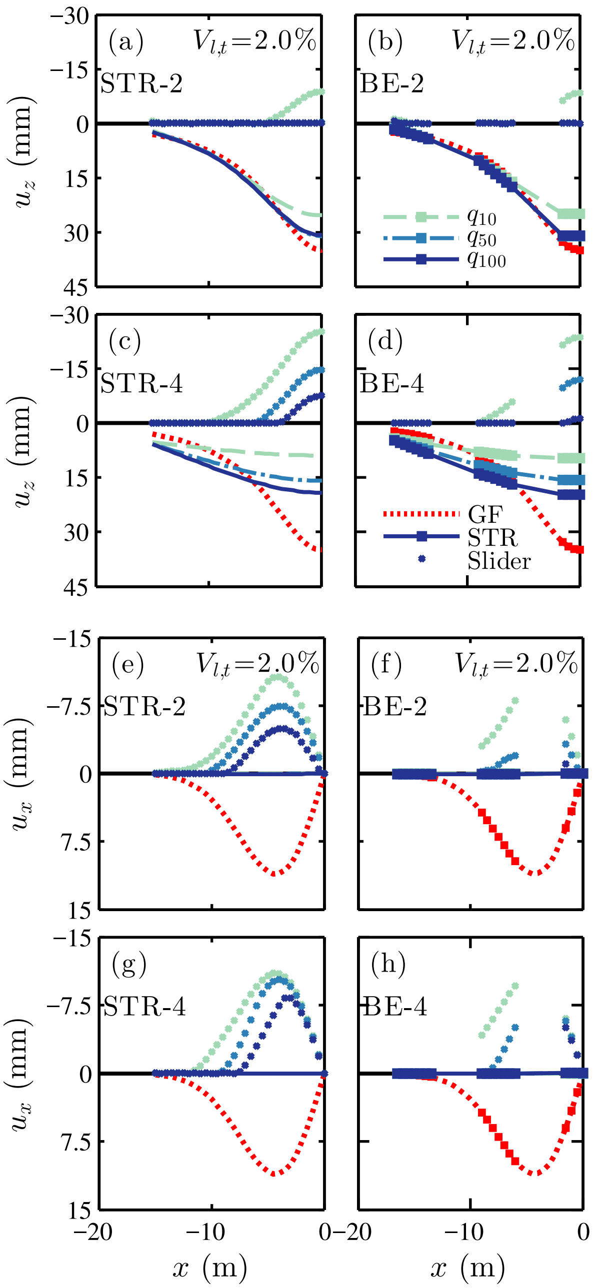

Fig. 7. Comparison of foundation displacements for structures STR and BE ($e/B = 0$).

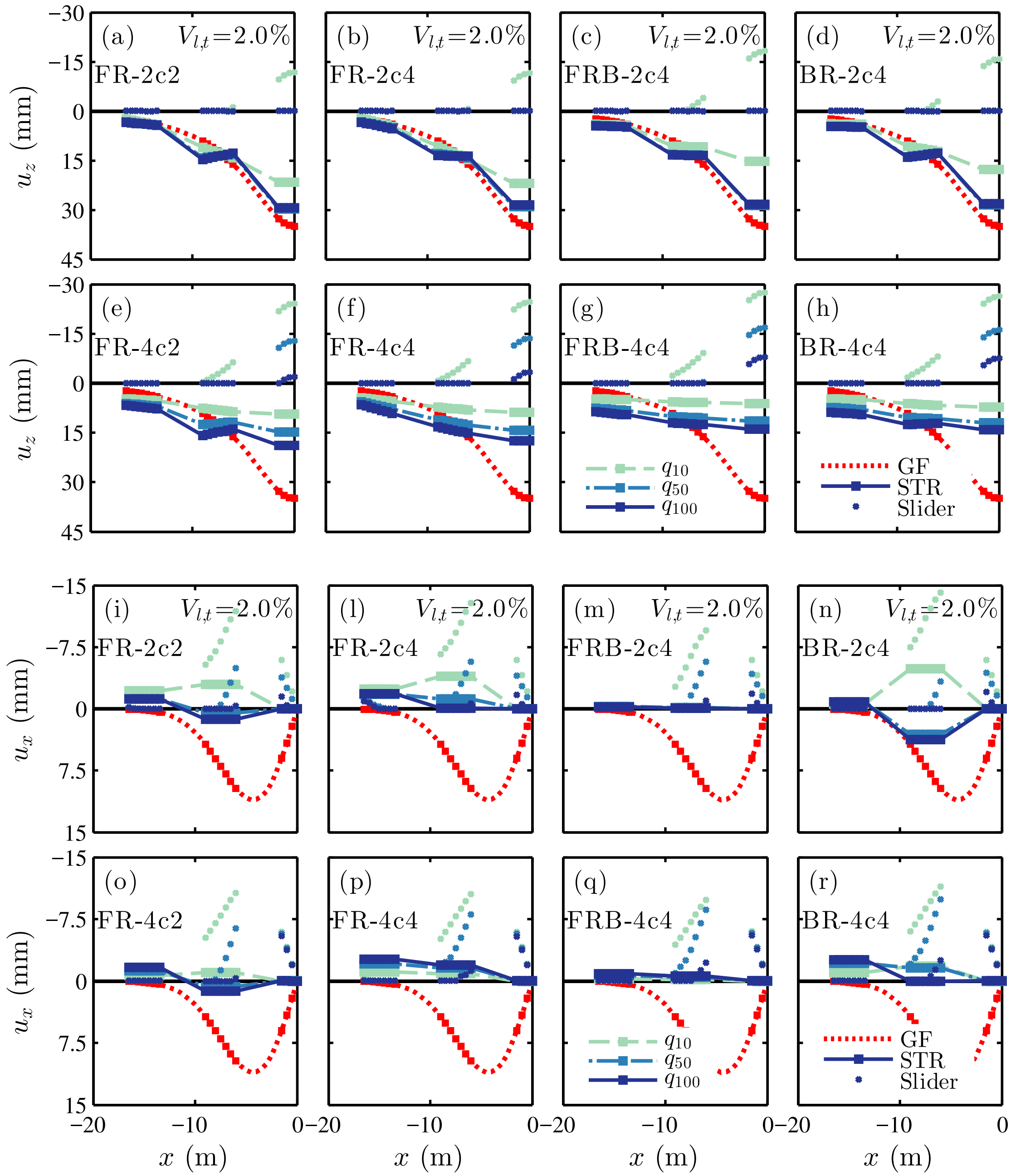

Fig. 8. Foundation displacements of framed structures on separated footings (e/B = 0).

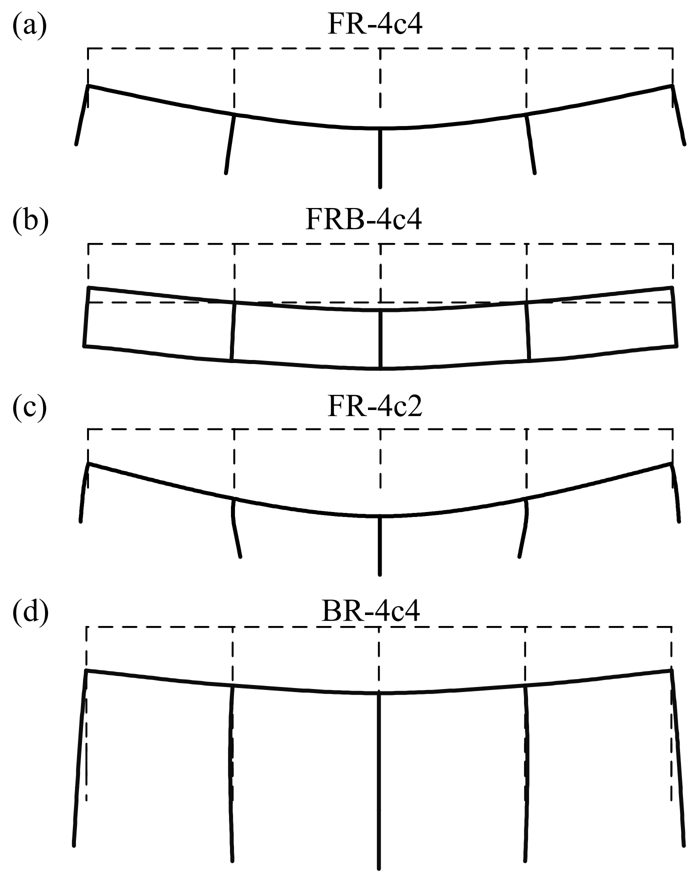

Fig. 9. Deformed shape of frames with $q_z = 100\text{kN/m}$ for centrally located tunnel and $V_{l,t} = 2‰$ (displacement factor: 250).

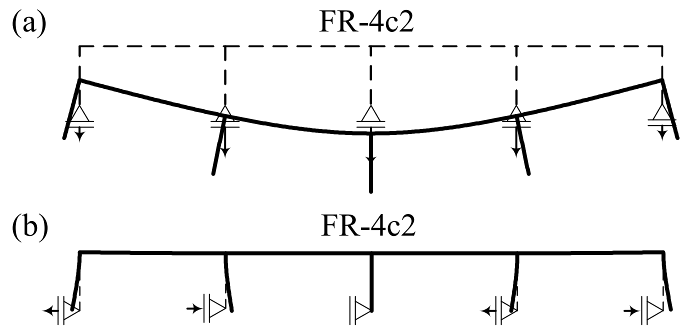

Fig. 10. Deformed shape of frame FR-4c2 to (a) vertical and (b) horizontal base displacements shown in Figure 9(c) (displacement factor: 250).

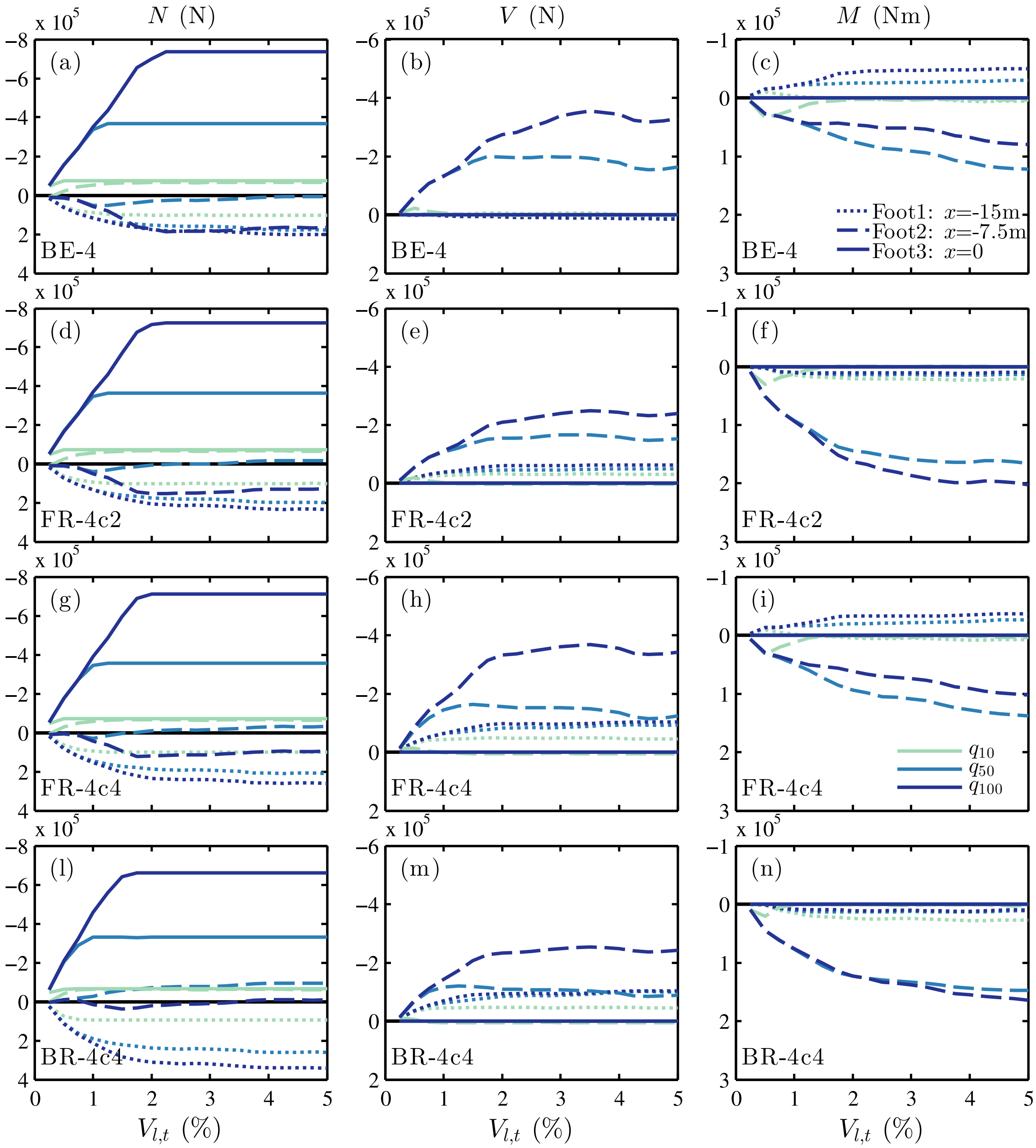

Fig. 11. Load transfer mechanism against tunnel volume loss for $e/B = 0$: effects of structural configuration and load condition.

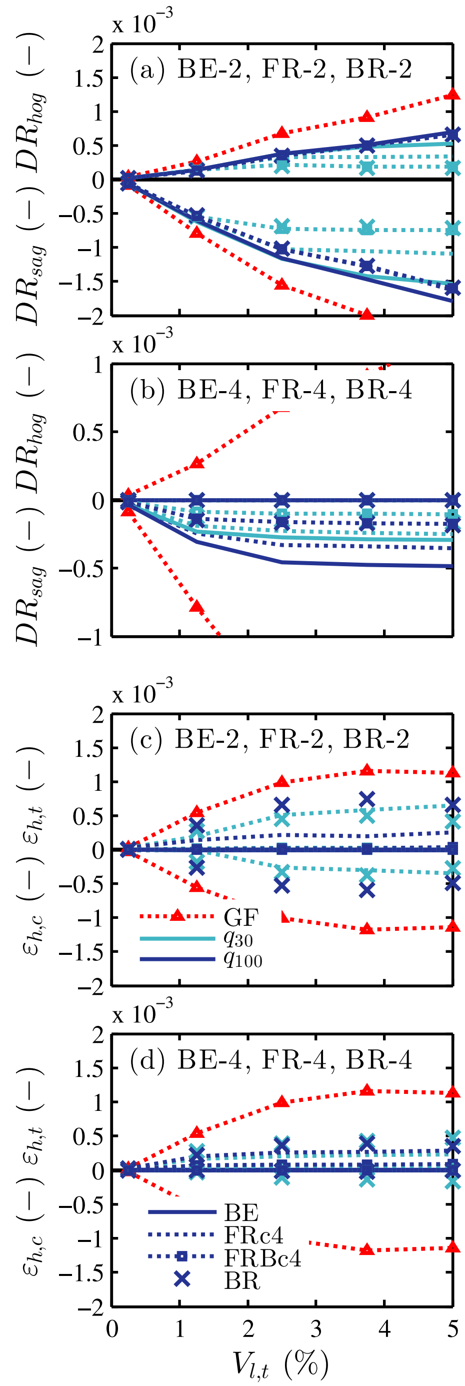

Fig. 12. Maximum deformation parameters associated with greenfield movements profiles and foundation displacements.

SUPPLEMENTAL DATA

List of Figures

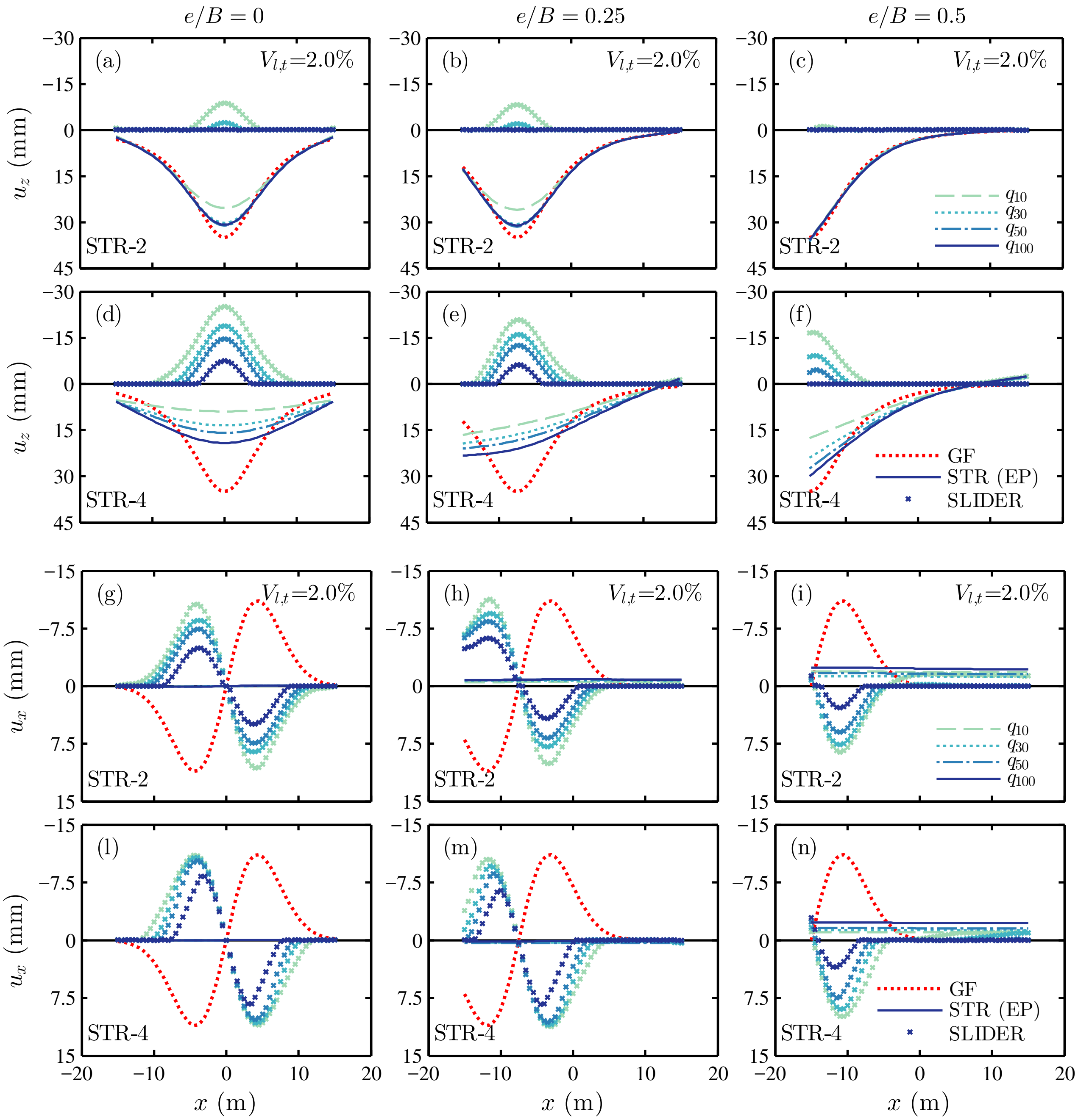

Fig. S1. Effects of tunnel eccentricity on displacements as well as gap and slippage.

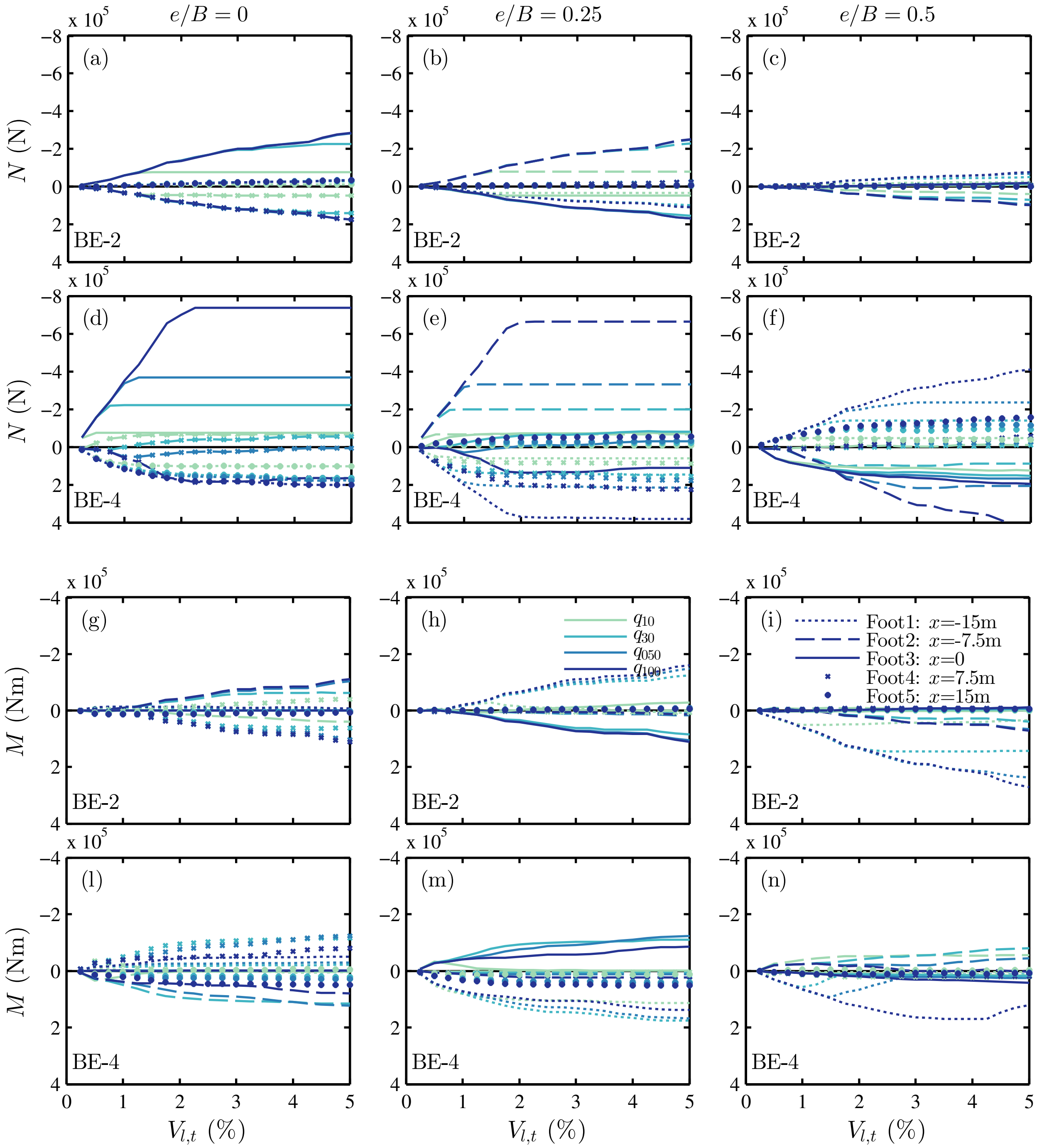

Fig. S2. Load transfer mechanism against tunnel volume loss of simple beams on separated footings: influence of tunnel-structure eccentricity and tunnel eccentricity.

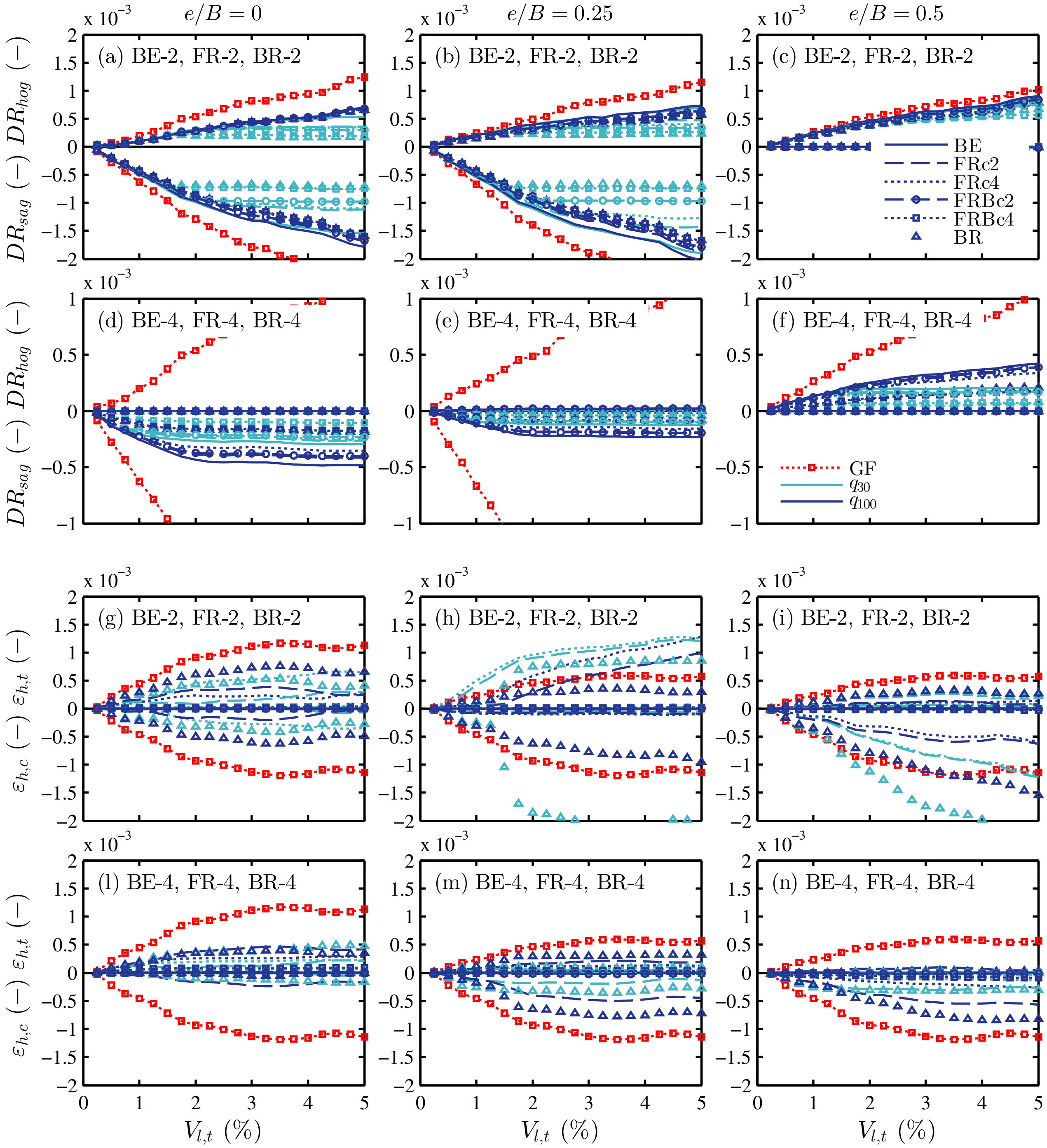

Fig. S3. Maximum deformation parameters associated with greenfield movements profiles and foundation displacements.